

Scalar absorption by particles advected in a turbulent flow

A. Sozza,^{1,*} M. Cencini,^{1,†} F. De Lillo,² and G. Boffetta²

¹*Istituto dei Sistemi Complessi, CNR, via dei Taurini 19,
00185 Rome, Italy and INFN, sez. Roma2 “Tor Vergata”*

²*Dipartimento di Fisica and INFN, Università di Torino, via P. Giuria 1, 10125 Torino, Italy.*

(Dated: October 14, 2021)

We investigate the effects of turbulent fluctuations on the Lagrangian statistics of absorption of a scalar field by tracer particles, as a model for nutrient uptake by suspended non-motile microorganisms. By means of extensive direct numerical simulations of an Eulerian-Lagrangian model we quantify, in terms of the Sherwood number, the increase of the scalar uptake induced by turbulence and its dependence on the Peclet and Reynolds numbers. Numerical results are compared with classical predictions for a stationary shear flow extended here to take into account the presence of a restoring scalar flux. We find that mean field predictions agree with numerical simulations at low Peclet numbers but are unable to describe the large fluctuations of local scalar uptake observed for large Peclet numbers. We also study the role of velocity fluctuations in the local uptake by looking at the temporal correlation between local shear and uptake rate and we find that the latter follows fluid velocity fluctuations with a delay given by Kolmogorov time scale. The relevance of our results for aquatic microorganisms is also discussed.

* Corresponding author; asozza.ph@gmail.com

† Corresponding author; massimo.cencini@cnr.it

I. INTRODUCTION

Mass or heat transfer in multi-phase systems is a problem of great interest for both theory and applications. Several industrial processes involve fluids with suspended particles that undergo chemical reactions, where particles exchange mass or heat with the surrounding fluid [1–3]. Fluid flows also mediate the uptake of nutrients and other biochemicals by suspended (unicellular) microorganisms [4, 5]. Previous works have shown that small-scale turbulence enhances the transport of nutrients into the cell [4, 6]. Such increase in the nutrient flux is typically negligible for bacteria while it can be significant for larger cells such as eukaryotic phytoplankton. However, these studies have considered turbulence as an average, time independent, shear flow while velocity and scalar fields in turbulent flows exhibit strong fluctuations and develop large gradients that are completely overlooked by a mean field description [7]. Consequently, the effects of turbulent fluctuations and their intermittency on cellular uptake are largely unknown. By stirring the nutrient patches, turbulence creates inhomogeneities and complex landscapes of nutrient [8] that make the uptake problem non-trivial. Moreover, the variability induced by small-scale turbulence may affect the ecological strategies in terms of growth and reproduction rates [9].

Previous numerical simulations have studied the problem of cellular uptake using different approaches. For instance, continuous (Eulerian) models for describing the concentration of both nutrients and (a population of) absorbers have been used for studying phytoplankton dynamics [10, 11] and for quantifying the interaction between motility and turbulence in bacterial chemotaxis [12, 13], but do not provide information on the uptake by a single particle. Discrete, Lagrangian models have also been used for computing the uptake of nutrient in a still fluid or in simple laminar flows [14, 15], thus disregarding the unsteadiness of turbulent flows.

In this work, we numerically study the effects of turbulent fluctuations on nutrient uptake by using a mixed Lagrangian-Eulerian approach. The nutrient is represented by a continuous, passive scalar field, while the absorbers are represented by Lagrangian particles. Both the nutrient and the absorbers are transported by a realistic turbulent flow obtained by the integration of the Navier-Stokes equations at high resolution. Scalar absorption is implemented by volumetric sinks centered at the particle positions, which has been shown to give accurate results in the absence of a flow or in simple laminar flows [16]. In order to maintain a statistically stationary state in a finite volume, nutrient is replenished by a uniform source (a chemostat, which models the upwelling from a nutrient rich reservoir [10, 17]). For an accurate comparison with simulations, we extend the analytical results of the uptake enhancement by a shear flow [18] to the presence of a restoring

flux.

The remaining of the manuscript is organized as follows. In Sec. II, we introduce the model and briefly describe the analytical derivation of nutrient uptake in the presence of a uniform restoring source. In Sec. III, we summarize the numerical implementation of the model and the parameters used in the simulations. In Sec. IV, we discuss the numerical results and their comparison with the analytical prediction based on the mean field model. Finally, Section V is devoted to conclusions and discussions. The appendices detail the analytical results.

II. MATHEMATICAL MODELS AND THEORETICAL RESULTS

A. Model equations

We consider the general problem of N discrete particles – the absorbers – transported by an incompressible velocity field $\mathbf{u}(\mathbf{x}, t)$ together with a passive scalar field $c(\mathbf{x}, t)$ – the nutrient concentration. Particles are considered as point tracers whose position \mathbf{X}_i evolves according to

$$\dot{\mathbf{X}}_i = \mathbf{u}(\mathbf{X}_i, t), \quad i = 1, \dots, N. \quad (1)$$

The velocity field is a solution of the incompressible Navier-Stokes equation

$$\partial_t \mathbf{u} + \mathbf{u} \cdot \nabla \mathbf{u} = -\nabla p + \nu \Delta \mathbf{u} + \mathbf{f}, \quad (2)$$

where ν is the kinematic viscosity, p the pressure and \mathbf{f} a body forcing injecting energy at rate ε on average equal to the energy dissipation rate, so to establish a statistically steady turbulent state. The nutrient is advected by the flow, diffuses with diffusivity D , is absorbed by the particles and uniformly restored at a rate μ to maintain, on average, a constant concentration c_0 ; its evolution reads

$$\partial_t c + \mathbf{u} \cdot \nabla c = D \Delta c - \sum_{i=1}^N \beta_i \delta(\mathbf{x} - \mathbf{X}_i) c - \mu(c - c_0). \quad (3)$$

In applications to plankton into the ocean, the uniform nutrient flux models the vertical advection from a deep reservoir – a chemostat – with constant concentration [17]. Following Ref. [16], absorption from the i^{th} particle is modeled through a volumetric absorption rate, β_i , and not via absorbing boundary conditions at the particle surface. According to this model, the instantaneous uptake of i^{th} particle is given by

$$\kappa_i(t) = \int d^3 \mathbf{x} \beta_i \delta(\mathbf{x} - \mathbf{X}_i) c(\mathbf{x}, t). \quad (4)$$

The numerical implementation of this model has been calibrated and tested by using configurations of one, two or more absorbers in still fluid and a laminar shear flow for which analytical results are available [16]. Our main interest here is to quantify the effect of turbulence on the uptake rate at the level of the single particle. Specifically, by denoting with κ_μ the asymptotic uptake rate obtained with the same chemostat but in the absence of the flow (i.e. when only diffusion is at play), we aim at quantifying the statistics of instantaneous Sherwood number, defined as $\text{Sh}(t) = \kappa_i(t)/\kappa_\mu$ and its average, and how they depend on the relevant parameters of the problem.

In the absence of a flow (see App. A), the effect of the chemostat is to exponentially cut-off the modification of the concentration field with a *screening length* $\xi = \sqrt{D/\mu}$, therefore reducing diffusive interactions between particles that without the chemostat are long ranged. As a consequence, the usual Smoluchovsky rate at $\mu = 0$, $\kappa_s = 4\pi DRc_0$, for an absorbing spherical particle of radius R is modified into Eq. (A3), which we rewrite here

$$\kappa_\mu = \kappa_s(1 + R/\xi). \quad (5)$$

By inverting (5), we obtain that a particle absorbing the nutrient with rate κ_μ has radius

$$R = \frac{\xi}{2} \left(\sqrt{1 + \frac{\kappa_\mu}{\pi D \xi c_0}} - 1 \right), \quad (6)$$

which can be used to define an effective radius for the point-particle model.

The instantaneous particle Peclet number, quantifying the importance of advection by the flow over diffusive transport, is then defined as $\text{Pe}(t) = \gamma R^2/D$ where $\gamma(t)$ measures the instantaneous turbulent shear rate at the particle position defined as $\gamma = (2S^2)^{1/2}$, where $S_{ij} = \frac{1}{2}(\partial_i u_j + \partial_j u_i)$ is the symmetric velocity gradient tensor at the particle position. It is useful to consider also the nominal Peclet number $\text{Pe}_\eta = \gamma_\eta R^2/D$ where $\gamma_\eta = 1/\tau_\eta$ is the inverse of the Kolmogorov time $\tau_\eta = (\nu/\varepsilon)^{1/2}$. We remark that, since γ is a concave function of the energy dissipation rate, due to Jensen inequality we have $\langle \gamma \rangle \leq \gamma_\eta$ and therefore $\langle \text{Pe} \rangle \leq \text{Pe}_\eta$. We also notice that, by introducing the Schmidt number $\text{Sc} = \nu/D$ and the Kolmogorov length $\eta = (\nu^3/\varepsilon)^{1/4}$, the nominal Peclet number can be expressed as $\text{Pe}_\eta = (R/\eta)^2 \text{Sc}$. The latter expression shows that, since the model requires $R \leq \eta$, the maximum attainable value of Pe_η is given by Sc . In the following, with some abuse of notation, when there is no ambiguity, we will often indicate the average Peclet and Sherwood numbers as Pe and Sh , respectively.

B. Theory of nutrient uptake in the presence of a chemostat

Classical results on the effect of a flow on nutrient uptake, obtained assuming a constant concentration at infinity, predict two different regimes for small and large Pe [6],

$$Sh = \begin{cases} 1 + 0.28 Pe^{1/2} & Pe \ll 1 \\ 0.55 Pe^{1/3} & Pe \gg 1 \end{cases} \quad (7a)$$

$$(7b)$$

obtained respectively assuming a linear shear flow with a point sink [18, 19] and making use of boundary-layer theory [18, 20]. In the following, we briefly show how the small Pe result (7a) can be generalized to the presence of a chemostat, details of the computation can be found in Appendix B. Note that the computation is based on a constant shear flow so that Pe should be interpreted as the average Peclet number, which in this case coincides with the instantaneous one.

We consider the concentration field $c(\mathbf{r}, t)$ relative to the center of a particle of radius R . The boundary conditions are $c(R, t) = 0$ (perfect absorption on the particle surface) and $\lim_{r \rightarrow \infty} c(\mathbf{r}, t) = c_0$. The main effect of the velocity field \mathbf{u} is to change the uptake rate by deforming the shape of the concentration profile with respect to the purely diffusive case. Following Ref. [18], we consider a particle smaller than the smallest scale in the flow (i.e. $R < \eta$), so that the velocity field around it can be expressed as a linear shear. We decompose the concentration field into a mean profile and a fluctuating one $c'(\mathbf{r}, t)$ that represents the deviations from the diffusive, spherical symmetric solution

$$c(\mathbf{r}, t) = c_0 \left(1 - \frac{\kappa(t)}{4\pi D r c_0 (1 + R/\xi)} e^{-(r-R)/\xi} \right) + c'(\mathbf{r}, t) \quad (8)$$

where $\kappa(t)$ represents the total (still unknown) flux to the particle.

In the absence of a flow ($\mathbf{u} = 0$) we have $c' = 0$ and $\kappa = \kappa_\mu$, as given by Eq. (5). In the presence of a flow, the relative increase of nutrient uptake, given by the Sherwood number $Sh(t) = \kappa(t)/\kappa_\mu$, is readily obtained imposing the condition $c(R, t) = 0$ in (8) which gives $Sh(t) = 1 + c'(R, t)/c_0$. The asymptotic (and here averaged) value of the Sherwood number, in the limit $t \rightarrow \infty$ can be obtained by extending the analysis of [18], which for $Pe \ll 1$ yields (see App. A for details)

$$Sh = 1 + \chi(\alpha) Pe^{1/2} \quad (9)$$

where

$$\chi(\alpha) = \frac{1}{(4\pi)^{1/2}} \int_0^\infty dz e^{-\alpha z} \frac{\sqrt{z}}{24 + z^2}, \quad (10)$$

Run	M	μ	ν	E	U	T	τ_η	L	η	ℓ_B	ξ	Re_λ	Sc	α_η
A1	128	0.2	1.6×10^{-2}	0.59	0.63	5.9	0.40	3.70	0.08	0.025	0.089	38	10	0.08
A2	256	0.2	6.4×10^{-3}	0.65	0.66	6.5	0.25	4.28	0.04	0.013	0.057	66	10	0.05
A3	512	0.2	2.5×10^{-3}	0.67	0.67	6.7	0.16	4.48	0.02	0.006	0.035	109	10	0.03
A4	512	0.3	2.5×10^{-3}	0.67	0.67	6.7	0.16	4.48	0.02	0.006	0.028	109	10	0.05
B1	128	0.2	6.4×10^{-3}	0.64	0.65	6.4	0.25	4.18	0.04	0.04	0.179	65	1.0	0.05
B2	1024	0.2	3.9×10^{-4}	0.70	0.68	7.0	0.06	4.78	0.005	0.005	0.045	287	1.0	0.01

TABLE I. Simulation parameters: Run index, resolution M , chemostat rate μ , kinematic viscosity ν , energy $E = \langle |\mathbf{u}^2| \rangle / 2$, rms velocity $U = (2E/3)^{1/2}$, integral times scale $T = E/\varepsilon$, Kolmogorov time scale $\tau_\eta = (\nu/\varepsilon)^{1/2}$, integral length scale $L = UT$, Kolmogorov length scale $\eta = (\nu^3/\varepsilon)^{1/4}$, Batchelor length scale $\ell_B = \eta/\text{Sc}^{1/2}$, screening length $\xi = (D/\mu)^{1/2}$, shear rate $\gamma_\eta = 1/\tau_\eta$, Taylor Reynolds number $\text{Re}_\lambda = U^2(15/\nu\varepsilon)^{1/2}$, Schmidt number $\text{Sc} = \nu/D$, and $\alpha_\eta = \mu\tau_\eta$. In all runs the energy injection rate is fixed at $\varepsilon = 0.1$, and $k_f = 1.5$.

with $\alpha = \mu\tau_\eta$ the relative time scale between stirring and nutrient supply. For $\alpha = 0$, Eq. (10) recovers Batchelor's result, $\chi(0) = \sqrt{\pi}/(6^{1/4}4) \simeq 0.283$. For $\alpha > 0$ the function decreases with α , meaning that the effect of the chemostat is to reduce the contribution of stirring to the nutrient uptake. This is somehow expected since with a fast chemostat (with $\alpha = O(1)$) the nutrient around the particle is uniformly restored before the flow deforms the iso-concentration surfaces.

III. DIRECT NUMERICAL SIMULATIONS

We solve Eqs. (2-3) via direct numerical simulation (DNS) on a triply periodic cubic domain of side $\mathcal{L} = 2\pi$ using up to $M^3 = 1024^3$ grid points with a 2/3 dealiased pseudo-spectral solver and 2nd order Runge-Kutta time marching. The forcing in Eq. (2), acting only at large scales (in the wave number shell $k \leq k_f$), is chosen in such way as to maintain the energy input ε constant. This is obtained by taking $\mathbf{f}(\mathbf{x}, t) = \varepsilon \mathbf{u}(\mathbf{x}, t) / 2E_{k \leq k_f} \Theta(k_f - k)$, where Θ is the Heaviside step function and $E_{k \leq k_f}$ the kinetic energy restricted to the wavenumbers $\leq k_f$ [21, 22]. We ensure that small-scale fluid motion is well resolved by imposing the Batchelor length scale $\ell_B = \eta/\sqrt{\text{Sc}}$ (the smallest scale in the problem since $\text{Sc} \geq 1$) to be at least of the same order of the grid spacing, ($k_{\max}\ell_B > 1.0$, where $k_{\max} = M/3$ is the maximum wave number available after dealiasing). The velocity field is integrated until a statistically stationary state is reached, then the concentration field is initialized to the constant value c_0 . We explored a range of Taylor-scale Reynolds number ($\text{Re}_\lambda \approx 38 - 287$) with two choices of the Schmidt number ($\text{Sc} = 1, 10$). Table I summarizes the main DNS parameters.

As for the solid phase, we seed N particles uniformly in the domain and let them move according to Eq. (1). The fluid velocity and its gradients (needed to estimate the shear rate) at particle positions are obtained via a 3^d order interpolation scheme. The δ -function in Eq. (3) is regularized by a function $f(\mathbf{x})$ with compact support, product of three functions of a single variable

$$f(\mathbf{x}) = \frac{1}{\Delta^3} \phi(x) \phi(y) \phi(z) \quad (11)$$

where $\Delta = \mathcal{L}/M$ is the grid size. The function ϕ is chosen to be symmetric, positive, normalized and with compact support around its center. One convenient form, used in the present work, is $\phi(x) = (1/n)[1 + \cos(2\pi x/(n\Delta))]$ for $|x| \leq n\Delta/2$ with $n = 4$ [23]. The uptake κ_i of each particle is then computed from (4) with the δ -function replaced by $f(\mathbf{x})$. More details can be found in [16].

In order to explore different values of the Peclet number, we selected different effective radii of the particles by tuning the absorption rate β . In particular, the radius is calibrated by performing, for each set of parameters, a diffusive simulation without flow and with static particles. For each β , the asymptotic uptake rate κ_μ is measured and Eq. (6) is used to define the particle radius [16].

To optimize the computational costs, several particles were integrated in each run. We remark that, in general, the presence of many particles in a finite domain induces diffusive interactions which tend to reduce the single particle uptake rate [16, 24, 25]. Although this effect is relevant to and interesting for applications [26, 27], in this work we focus on the single particle absorption, and therefore on dilute concentrations such that diffusive interactions are negligible. In this respect, the chemostat, inducing a screening length ξ , reduces the interactions among particles.

We can exploit the knowledge of the screening length to estimate the number of particles to be used to minimize the diffusive interactions. The flow being incompressible, the particle distribution remains uniform. By assuming a random uniform distribution of N particles in a cube domain of side \mathcal{L} , the probability density function (PDF) of nearest-neighbors distance, for small r takes the form [28]

$$P(r) = 4\pi r^2 \rho \exp\left(-\frac{4}{3}\pi r^3 \rho\right). \quad (12)$$

The mean inter-particle distance is $\langle r \rangle = a/\rho_p^{1/3}$, with $a = \Gamma(1/3)/(36\pi)^{1/3}$, where $\rho_p = N/\mathcal{L}^3$ is the particle number density. By choosing, e.g., $\langle r \rangle = 8\xi$ one has that the probability to find two particles at distance less than 2ξ is only 1%.

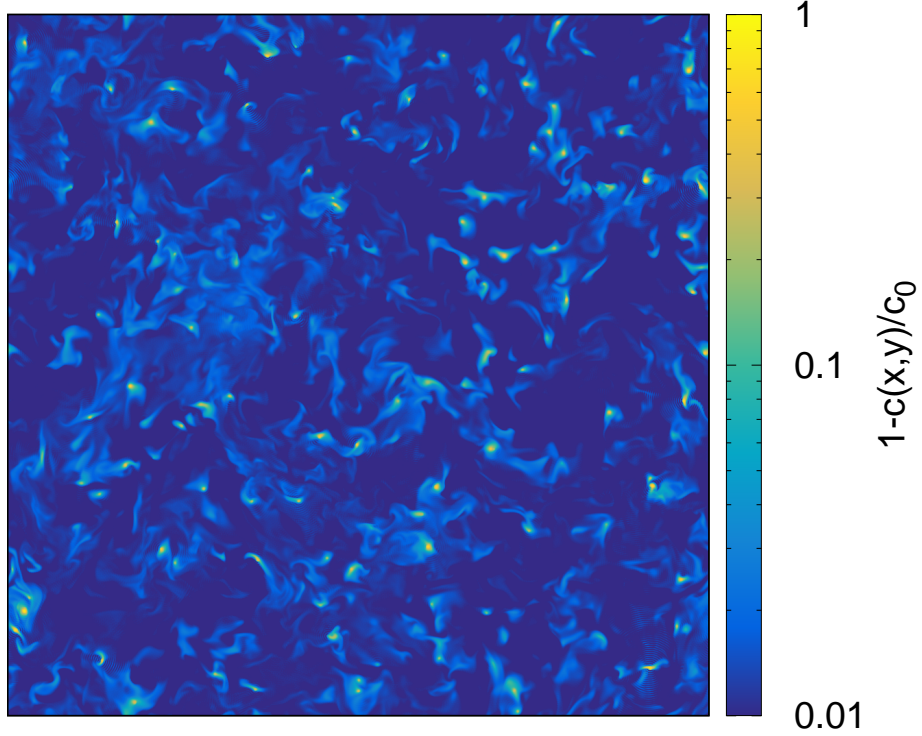


FIG. 1. (color online) Fluctuations of the concentration field $1 - c(\mathbf{x}, t)/c_0$ in a two-dimensional slab of 16 grid points. Resolution $M = 1024$ (Run B2).

IV. RESULTS

We start by showing in Fig. 1 a typical example of the concentration field in a two-dimensional section of the computational box. Due to the absorption, small depletion zones are created around the particles, which are then stretched by turbulence leading to filament-like structures. The presence of these structures reflects how turbulence locally increases scalar gradients, thus impacting particle uptake.

In Fig. 2, we plot the PDF of the shear rate γ for different values of the Reynolds number Re_λ . The form of this distribution has been widely studied in previous works and is characterized by non-Gaussian tails [29, 30], which become wider and wider at increasing Re_λ , the hallmark of intermittency in the statistics of the velocity gradients.

Strong gradients are expected to cause local modification of the absorption. Indeed variations of γ along the particle path modify the instantaneous value of the Peclet number. To understand and characterize these variations and their effect on the uptake we measure the instantaneous individual uptake κ , by using Eq. (4), and shear rate γ along each particle trajectories, in this

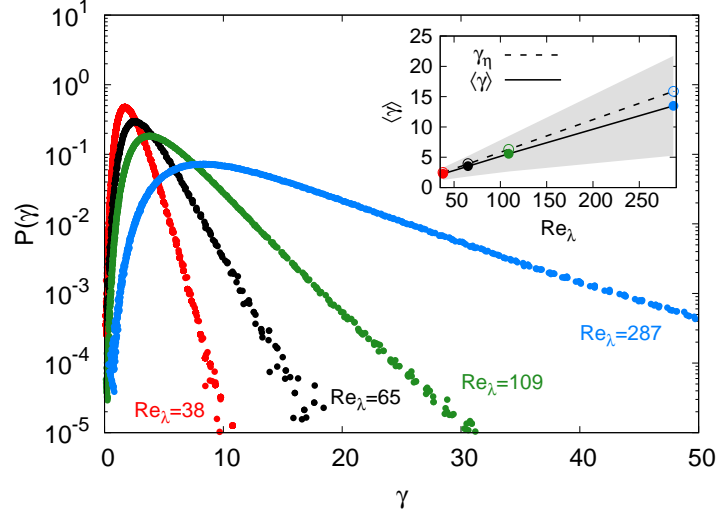


FIG. 2. (color online) Probability density function of shear rate $\gamma = (2S^2)^{1/2}$ for different Re_λ . Inset: mean shear rate $\langle\gamma\rangle$ (filled circles with solid line) and its root mean square (area in gray) compared with the dimensional estimation $\gamma_\eta = \tau_\eta^{-1}$ (empty circles with dashed line), due to the Jensen inequality $\langle\gamma\rangle < \gamma_\eta$.

way we can compute the local Peclet and Sherwood numbers. In Fig. 3, we plot the instantaneous value of $Sh - 1$, i.e. the deviation from the diffusive uptake induced by turbulence, as a function of Pe for particles with 9 different radii (each represented by a different color) transported by a turbulent flow at $Re_\lambda = 109$. Although a clear correlation between uptake rate and local shear is observed, as indeed the solid line shows that at changing the local Peclet number the Sherwood number changes according to the prediction valid for the average, we also observe large fluctuations of these values on a single particle (i.e. at fixed R).

The average values of the Peclet number $\langle Pe \rangle$ and of the Sherwood number $\langle Sh \rangle$ for the different simulations are shown in Fig. 4a together with the classical theoretical prediction (7a). Averages are computed over all particles having the same size and over time. Different symbols code the runs summarized in Table I. The $\langle Pe \rangle^{1/2}$ behavior of Eq. (7a) is clearly observable for small values of $\langle Pe \rangle$. We do not observe the $\langle Pe \rangle^{1/3}$ scaling of Eq. (7b), which is expected at larger $\langle Pe \rangle$, however the points at largest $\langle Pe \rangle$ of run A1 show a transition to a flatter scaling. As one can see, while the scaling Eq. (7a) is well reproduced, data obtained with different values of μ and Re_λ are not on the same master curve. The reason for this is the presence of the chemostat that modifies the constant in front of the $\langle Pe \rangle^{1/2}$ scaling. In Figure 4b we plot the Sherwood number rescaled with the coefficient $\chi(\alpha)$ (with $\alpha = \mu\tau_\eta$) given by (10), which generalizes Batchelor's result (corresponding to $\alpha = 0$). As one can see, now we find a good collapse for all the runs characterized by different values of Re_λ and α . For $\langle Pe \rangle \lesssim 0.5$, the analytical prediction (9) provides an accurate description

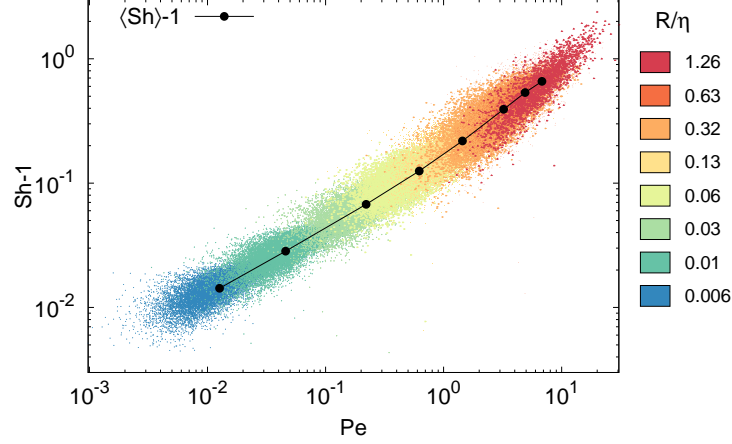


FIG. 3. (color online) Local gain of Sherwood number $\text{Sh} - 1$ versus local Peclet number Pe computed on the different particles of run A3, see Table I. Colors refer to 9 different values of the particles radius R as in label. The solid line with filled circles represents the behavior of $\langle \text{Sh} \rangle - 1$ versus $\langle \text{Pe} \rangle$.

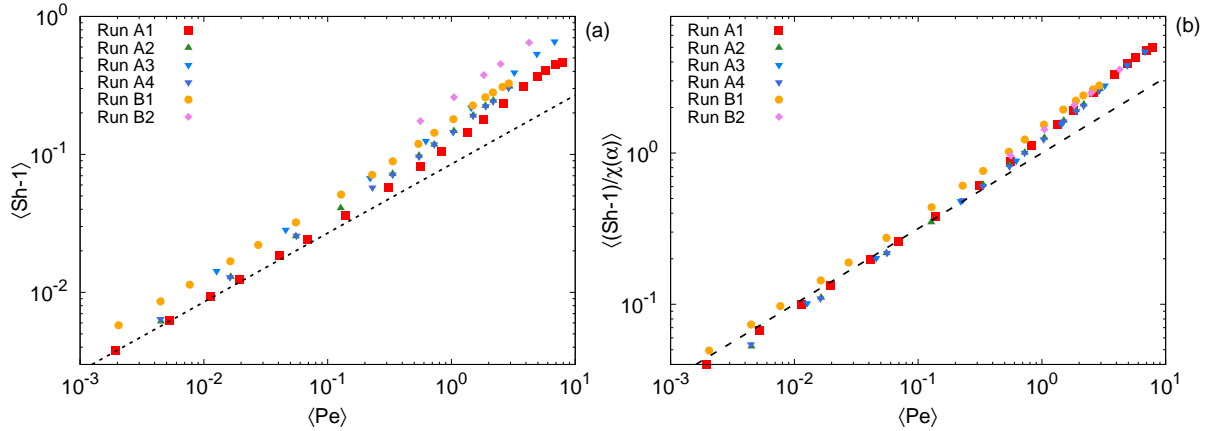


FIG. 4. (color online) Dependence of the mean Sherwood number on the mean Peclet number: (a) $\langle \text{Sh} \rangle - 1$ vs $\langle \text{Pe} \rangle$ for all runs. Average is taken over all the particles with the same radius and over time, after discarding a transient. The dashed line displays the $\langle \text{Pe} \rangle^{1/2}$ behavior of Eq. (7a). (b) $\langle \text{Sh} \rangle - 1$ rescaled by the coefficient $\chi(\alpha)$, see Eq. (10). The dashed line represents the prediction (9).

of the effect of turbulence on the uptake, which is mainly controlled by the Peclet number. We observe also some small difference between runs A and B, indicating a possible dependence on the Schmidt number which is not fully captured by the theoretical analysis. Remarkably, the collapse of the different curves is observed for all the available values of $\langle \text{Pe} \rangle$, even beyond the range of validity of (9).

Given the intense fluctuations that characterize turbulent gradients, we expect the local uptake rate to be subjected to strong variations with respect to the mean. In order to characterize those

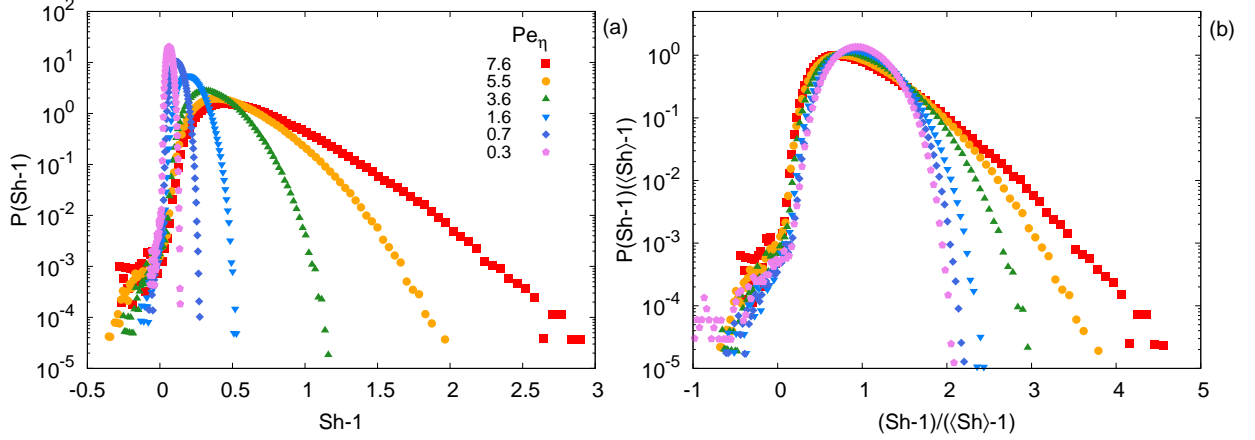


FIG. 5. (color online) PDF of the instantaneous Sherwood number Sh at varying the nominal Pe_η number, i.e. for various particle radius: (a) Pdf of the deviation $Sh - 1$ of the Sherwood number from the diffusive value. Curves are plotted for different Pe_η and fixed $Re_\lambda = 109$, $Sc = 10$ and $\alpha = 0.05$ (run A3). (b) the same PDF of panel (a) normalized by their average. Note that the increased uptake by larger particles is also accompanied by more intense fluctuations.

fluctuations we study the PDF of the local Sherwood number Sh for different values of the control parameters Re_λ , Pe_η , Sc . In Fig. 5, the distribution of Sh is plotted, at fixed Re_λ , Sc and α , for different values of Pe_η obtained by changing the effective particle radius R . For very small values of Pe_η (hence, small R), the observed values of Sh are confined to a narrow interval around 1. This confirms that the local uptake rate by small particles is mildly influenced by turbulence both in terms of its average and of its fluctuations. Increasing Pe_η (and consequently, the particle radius), the distribution moves towards larger values of Sh and develops wider right tails. This change of shape in the distribution is made more evident in Fig. 5b, where the PDFs are normalized with the average value $\langle Sh \rangle$. The small left tails for $Sh < 1$ are due to the diffusive interactions among the particles in the simulation box. The relative importance of this effect is consistent with the estimation based on the particle number with random distribution and could, in principle, be eliminated by decreasing the number of particles. Nonetheless, the effect is very small and does not affect the global shape of the PDF.

In order to directly scrutinize the effect of increasing turbulent mixing, we now fix the particle size, i.e. the nominal Peclet number, and consider different values of Re_λ . In Figure 6a, we show the PDF of Sh for three cases in which the nutrient replenishment rate μ of the chemostat is kept constant while varying Re_λ . By definition, for fixed μ , α decreases as turbulence becomes more intense and this produces a shift of the PDF towards larger values of Sh . An increase in Re_λ ,

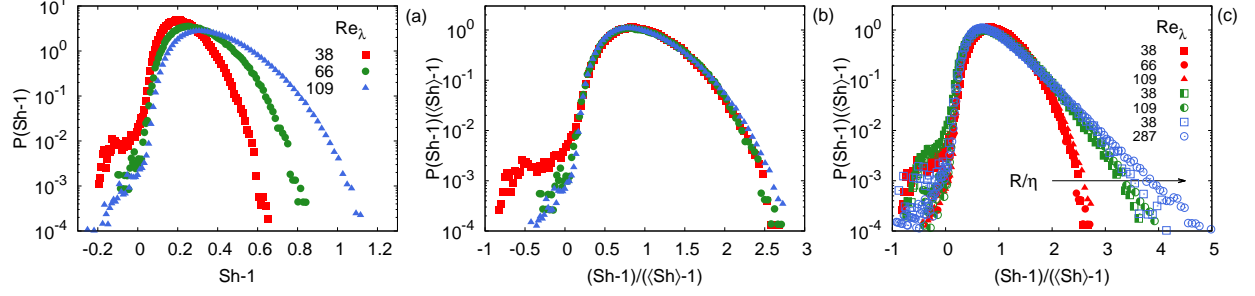


FIG. 6. (color online) PDF of $Sh - 1$ for different Re_λ : (a) holding fixed $Pe_\eta = 3$, $Sc = 10$. The chemostat rate μ is also fixed so that larger Re_λ corresponds to smaller α ; (b) same as (a), but normalizing the PDFs of $Sh - 1$ with their average value, demonstrating that, even though the average $\langle Sh \rangle$ increases with Re_λ , the shape of the distribution is not strongly affected by the turbulence intensity. (c) same rescaling as in (b) repeated for three sets of particles, with different radii, namely $R/\eta = \sqrt{Pe_\eta/Sc} = 0.57$ (red symbols), 0.87 (green symbols), 1.70 (empty symbols) respectively.

however, does not seem to affect the shape of the distribution, as one can appreciate from Fig. 6b, where the PDFs are normalized with their mean values. In these three cases both the nominal Peclet, Pe_η , and the Schmidt, Sc , numbers are kept constant, which physically speaking means that the ratio of the particle radius to the Kolmogorov length is also constant, as $R/\eta = \sqrt{Pe_\eta/Sc}$. In Fig. 6c, we show the PDFs for three different values of R/η . As one can see, the rescaled PDFs collapse fairly well, implying that R/η dominates the overall shape of the distributions, especially the behavior of the right tail, with more intense fluctuations in uptake measured when the effective radius reaches the Kolmogorov scale. Residual effects in Re_λ , however, cannot be completely ruled out. It is worth emphasizing that $R \sim \eta$ constitutes the upper limit for the particle size within our model, therefore the details of the statistics close to this limit should be taken with caution. However, the consistency of the behavior through about a factor three in radius seems to support the robustness of the observation.

We conclude by briefly discussing the relevance of time correlations in the uptake process. Indeed, it is reasonable to expect that a local fluctuation of the velocity gradient at a given time should produce a corresponding fluctuation in the scalar uptake with some delay time. This is qualitatively confirmed by inspecting the temporal signals of the instantaneous Sherwood and Peclet numbers, shown in Fig. 7a. In order to quantify this delay we compute the connected cross correlation between Pe and Sh normalized by their standard deviation, which is shown in Figs. 7(b) and (c) at varying the relevant parameters. As one can see, the correlation functions attain their maximum value for a delay time of the order of τ_η . The Kolmogorov times scale is

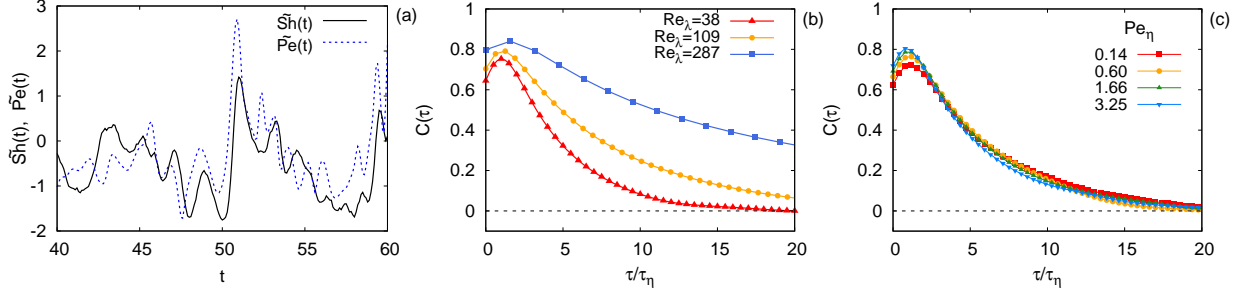


FIG. 7. (color online) Correlation between local strain and uptake rates: (a) Temporal signal of the normalized variables $\widetilde{Sh}(t) = (Sh(t) - \langle Sh \rangle) / \sigma_{Sh}$ (black solid line) and $\widetilde{Pe}(t) = (Pe(t) - \langle Pe \rangle) / \sigma_{Pe}$ (blue dashed line) for $Re_\lambda = 66$ (Run A2) and $Pe_\eta = 2$. (b) Temporal cross correlation $C(\tau) = \langle \widetilde{Pe}(t) \widetilde{Sh}(t + \tau) \rangle$ for different Re_λ (Run A1, A3 and B2) while taking $\mu = 0.2$ constant, thus changing α , with $Pe_\eta = 1$. Time is rescaled by τ_η to make clear that the maximum is attained at $\tau \approx \tau_\eta$. Without this rescaling the long time decay of the different curves is basically the same, meaning that it is mainly controlled by the chemostat rate μ (not shown). (c) for different Pe_η , as in label, at fixed $Re_\lambda = 66$ and $Sc = 10$ (for clarity, not all data points are represented).

indeed the time scale for the deformation of the nutrient field to take place around the particle in the viscous-diffusive regime of scalar transport, which is the one relevant to the problem [31].

V. CONCLUSIONS

In this work we have studied the effect of turbulence on the scalar uptake by spherical absorbing particles advected by the flow. By means of realistic, direct numerical simulations at different turbulent intensities, we computed the instantaneous absorption of a scalar field, and its gain with respect to a purely diffusive process. We used a point particle method with volumetric absorption of the nutrient scalar field calibrated to represent particles of different sizes (i.e. Peclet numbers).

The scalar uptake relative to a purely diffusive process, quantified by the Sherwood number Sh , is found to depend on the average particle Peclet number Pe , in agreement with classical predictions based on a mean-field representation of turbulence. Nonetheless, we observe strong fluctuations in the instantaneous and local value of Sh , whose PDF develops wide tails in particular for large values of Peclet (i.e. large radii) and Reynolds numbers.

By analyzing the time series of Sh and Pe along a particle trajectory, we observed a delay between the two signals which was quantified by computing the cross correlation function. This delay is found to be of the order of the Kolmogorov time of the flow and depends weakly on the Peclet number.

It is now worth discussing the possible relevance of our findings for the nutrient uptake by small non-motile microorganisms transported by fluid flows. In the ocean [32, 33], using as reference parameters $\varepsilon = 10^{-4} - 10^{-8} m^2 s^{-3}$, $\nu = 10^{-6} m^2 s^{-1}$, and $D \sim 10^{-9} m^2 s^{-1}$ (for the most important nutrient like phosphate and nitrate) one has $\tau_\eta = 0.1 - 10 s$ and $Sc = 10^3$. For a phytoplankton cell of size $R = 10^{-6} m$ (e.g., a bacterium), the Peclet number ranges between $Pe = 10^{-4} - 10^{-2}$ and, therefore, the effect of turbulence on nutrient uptake is expected to be negligible. Conversely, for cells of size $R = 10^{-4} m$ we have $Pe = 1 - 100$ and the average cellular uptake, according to our results, can be substantially affected by turbulence with an increase up to about two times with respect a purely diffusive environment [6]. In particular, our results show that, in this regime, the local value of the uptake can be much larger than the mean, with a PDF which develops very large tails. To the best of our knowledge, the effect of fast and strong nutrient fluctuations on phytoplankton growth is not known. Our findings suggest that it would be interesting to investigate this issue experimentally.

We also observe that the proposed model, besides being relevant to nutrient uptake of non-motile micro-organisms, is suitable to describe a variety of different applications, such as evaporation and condensation of droplets [34–36], in which the emission and absorption of supersaturated water vapor is mediated by turbulent transport.

The present analysis focused on the situation in which the nutrient is continuously replenished at all scales by a constant chemostat. While this can mimic nutrient upwelling from an underlying reservoir [17], other kinds of forcing may be relevant to real applications. For instance, injections which, unlike the chemostat here used, replenish the nutrient only at large scales. Preliminary tests (not shown) in this direction [37] indicate that the main findings of our analysis are robust. In particular, intense fluctuations in the local Sherwood number are observed independently on the forcing used, thus confirming the importance of a description that goes beyond the mean field approach.

Especially in the ocean, nutrient sources are often distributed in small ephemeral patches [38]. Thus, a natural extension of this model would be to consider a forcing for the nutrient not uniform in space and time, representing the variability present in nature. Other possible extensions of the model are in the direction of a better representation of the absorption mechanism which could take into account more accurately of the local effects of the flow such as, for example, rotation of the cell due to local vorticity and its effect on the uptake [39].

ACKNOWLEDGMENTS

We acknowledge HPC CINECA for computing resources (INFN-CINECA Grant No. INFN19-fldturb). F.D. acknowledges PRACE for awarding access to GALILEO at CINECA through project *LiLiPlaTE*. G.B. and F.D. acknowledge support by the Departments of Excellence grant (MIUR). A.S. acknowledges HPC CINECA for ISCRA-C Project *NUPhTu* as well as Italian research project MODSS (Monitoring Debris Space Stereo) Grant No. ID 85-2017-14966, funded by Lazio Innova (Regione Lazio) according to Italian law L.R. 13/08.

Appendix A: Smoluchowski rate in a chemostat

Consider a spherical particle immersed in a quiescent nutrient concentration $c(\mathbf{x}, t)$ sustained by a chemostat, i.e. ruled by the equation

$$\partial_t c = D\Delta c - \mu(c - c_0), \quad (\text{A1})$$

with initial condition $c(\mathbf{x}, 0) = c_0$ and boundary conditions $c(R, t) = 0$ at the surface of the sphere and $c(\infty, t) = c_0$, where we used the spherical symmetry of the problem. At stationarity, the relative concentration, $\psi = 1 - c/c_0$, satisfies the equation $\psi'' + 2\psi'/r - \mu\psi/D = 0$. Solving for the concentration yields

$$c(\mathbf{r}, t) = c_0 \left[1 - \frac{R}{r} e^{-(r-R)/\xi} \right], \quad (\text{A2})$$

where the long-range behavior of the solution without source term is exponentially damped with *screening length* $\xi = \sqrt{D/\mu}$. The uptake rate is obtained by integrating the nutrient flux $\mathbf{J} = -D\partial_r c$ over the surface of the sphere

$$\kappa_\mu = \oint \mathbf{J} \cdot \hat{\mathbf{n}} \, dS = \kappa_s \left(1 + \frac{R}{\xi} \right) \quad (\text{A3})$$

with $\kappa_s = 4\pi DRc_0$ being the usual Smoluchowski rate, which is recovered in the limit $\mu \rightarrow 0$ (i.e. $\xi \rightarrow \infty$).

Appendix B: Generalization of the Batchelor calculations for a chemostat

We report here the details of the analytical derivation of the Sherwood number behavior in the $\text{Pe} \ll 1$ limit, by following the work of Batchelor [18], and extending his result for the case of a chemostat.

We start by considering the equation for a nutrient concentration $c(\mathbf{x}, t)$, advected by the velocity field $\mathbf{u}(\mathbf{x}, t)$ and replenished by a chemostat with rate μ ,

$$\partial_t c + \mathbf{u} \cdot \nabla c = D \Delta c - \mu(c - c_0). \quad (\text{B1})$$

Absorption by the particle is modeled by the boundary conditions: $c = 0$ at the particle surface, i.e. for $r = R$ (where $r = |\mathbf{r}|$) and $c = c_0$ in the far away distance, $\mathbf{r} \rightarrow \infty$.

As a first approximation, we assume a time-independent linear shear flow, i.e. $u_i = G_{ij}x_j$, with $G_{ij} = \partial_j u_i$ constant. As usual, the gradient tensor G_{ij} can be written as $G_{ij} = S_{ij} + \Omega_{ij}$, with the symmetric, $S_{ij} = \frac{1}{2}(\partial_j u_i + \partial_i u_j)$, and anti-symmetric, $\Omega_{ij} = \frac{1}{2}(\partial_j u_i - \partial_i u_j)$, component representing straining motion and rigid-body rotation, respectively.

We begin by searching for a solution in Fourier space for the concentration field in the case of an instantaneous source with uptake rate κ . In order to study the mass transfer in the proximity of the particle, it is convenient to adopt the comoving coordinates $\mathbf{r} = \mathbf{x} - \mathbf{X}_i$. We also rewrite Eq. (B1) for the relative concentration $\psi = 1 - c/c_0$, with boundary condition $\psi(\infty, t) = 0$ and $\psi(R, t) = 1$. Considering the Fourier transform $\hat{\psi}(\mathbf{q}, t) = \int_{-\infty}^{\infty} \psi(\mathbf{r}, t) e^{-i\mathbf{q} \cdot \mathbf{r}} d^3\mathbf{r}$, Eq. (B1) reads

$$\frac{\partial \hat{\psi}}{\partial t} - G_{ij} q_i \frac{\partial \hat{\psi}}{\partial q_j} = -D q^2 \hat{\psi} - \mu \hat{\psi} \quad (\text{B2})$$

with $q = |\mathbf{q}|$.

The concentration field for a sustained source is obtained as the time integral of the solution of the instantaneous source, i.e.

$$\hat{\psi}(\mathbf{q}, t) = \kappa \int_0^t ds e^{-D q_i B_{ij} q_j - \mu s} \quad (\text{B3})$$

with $B_{ij}(t)$ a time-dependent symmetric matrix that incorporates the effects of the shear. In the absence of shear, it reduces to a diagonal matrix that describes isotropic diffusion with a Gaussian solution [40, 41]. Plugging the solution in Eq. (B2) yields the equation for the tensor B_{ij} that, after some algebra, reads

$$\frac{dB_{ij}}{dt} = \delta_{ij} + G_{il} B_{jl} + G_{jl} B_{il} \quad (\text{B4})$$

Now anti-transforming, the concentration field becomes

$$\psi(\mathbf{r}, t) = \kappa \int_0^t ds \int_{-\infty}^{\infty} \frac{d^3 \mathbf{q}}{(2\pi)^3} e^{i\mathbf{q} \cdot \mathbf{r} - D\mathbf{q} \cdot \mathbf{B} \mathbf{q} - \mu s}, \quad (\text{B5})$$

which can be easily solved by Gaussian integration, yielding in physical space,

$$\psi(\mathbf{r}, t) = \frac{\kappa}{(4\pi D)^{3/2}} \int_0^t \frac{ds}{\sqrt{\det(\mathbf{B})}} e^{-\mathbf{r} \cdot \mathbf{B}^{-1} \mathbf{r} / (4D) - \mu s}. \quad (\text{B6})$$

The steady state solution, which corresponds to the diffusive approximation around the absorbing particle, is obtained taking the limit $t \rightarrow \infty$, and approximating the integrand with its Taylor expansion in $r = 0$ and $s = 0$ [19]. At the lowest order we can assume $B_{ij} = s \delta_{ij}$, $\det(B_{ij}) = s^3$ and $B_{ij}^{-1} = s^{-1} \delta_{ij}$, obtaining

$$\bar{\psi}(r) \approx \frac{\kappa}{(4\pi D)^{3/2}} \int_0^\infty \frac{ds}{s^{3/2}} e^{-\frac{r^2}{4Ds} - \mu s} = \frac{\kappa e^{-r/\xi}}{4\pi D r} \quad (\text{B7})$$

The Sherwood number, defined as $\text{Sh}(t) = 1 + c'(R, t)/c_0$ is computed subtracting the steady state solution to the global solution as $c'(\mathbf{r}, t)/c_0 = \bar{\psi}(r) - \psi(\mathbf{r}, t)$. We then perform the average over time by taking the limit $t \rightarrow \infty$, and then evaluate the integral at particle surface by taking the limit $r \rightarrow 0$. Since κ differs weakly from κ_s , we can approximate the integral as

$$\text{Sh} = 1 + \frac{R}{(4\pi D)^{1/2}} \int_0^\infty \left(s^{-3/2} - \det(\mathbf{B})^{-1/2} \right) e^{-\mu s} ds \quad (\text{B8})$$

An approximation valid for a generic linear shear flows can be found by expanding B_{ij} as power series in t : $B_{ij} = \delta_{ij}t + B_{ij}^{(2)}t^2 + B_{ij}^{(3)}t^3 + \dots$. Hence, substituting in Eq. (B4) we can determine the first coefficients

$$\begin{aligned} B_{ij}^{(2)} &= \frac{1}{2}(G_{ij} + G_{ji}) = S_{ij} \\ B_{ij}^{(3)} &= \frac{2}{3}S_{il}S_{jl} + \frac{1}{3}(S_{il}\Omega_{jl} + S_{jl}\Omega_{il}) \end{aligned} \quad (\text{B9})$$

Now we consider the axes of reference to coincide with the principal axes of the rate of strain tensor S_{ij} to obtain a simple shear flow along a preferential direction $G_{12} = \gamma$, $S_{12} = S_{21} = \gamma/2$, so that Eq. (B9) is satisfied by

$$\begin{aligned} B_{11} &= t(1 + \frac{1}{3}\gamma^2 t^2), \quad B_{22} = t, \quad B_{33} = t \\ B_{12} &= \frac{1}{2}\gamma t^2, \quad B_{21} = B_{23} = B_{33} = 0. \end{aligned} \quad (\text{B10})$$

The determinant of B_{ij} is given by

$$\left(\frac{\det(\mathbf{B})}{t^3} \right)^{1/2} = 1 + \frac{\gamma^2 t^2}{24} \quad (\text{B11})$$

By changing variable to $s = z/\gamma$ and by defining the parameter $\alpha = \mu/\gamma$, the Sherwood number in the case of a generic linear shear flow and in the presence of a chemostat is then given by

$$\text{Sh} = 1 + \chi(\alpha)\text{Pe}^{1/2} \quad \text{with} \quad \chi(\alpha) = \frac{1}{(4\pi)^{1/2}} \int_0^\infty dz e^{-\alpha z} \frac{\sqrt{z}}{24 + z^2}. \quad (\text{B12})$$

The integral admits a real solution for $\alpha > 0$ and for $\alpha = 0$ it recovers the prediction given by Batchelor, $\chi(0) = \sqrt{\pi}/(6^{1/4}4)$ [18]. The parameter α is the ratio between the time-scale of

replenishment of the nutrient by the source and the stirring of fluid due to advection. Therefore, the nutrient source changes the rate of transfer and enters into the computation of the Sherwood number in a not trivial way.

-
- [1] P. Harriott, “A review of mass transfer to interfaces,” *Canad. J. Chem. Engin.* **40**, 60–69 (1962).
 - [2] P. Harriott, “Mass transfer to particles: Part i. suspended in agitated tanks,” *AIChE J.* **8**, 93–101 (1962).
 - [3] P. M Armenante and D. J Kirwan, “Mass transfer to microparticles in agitated systems,” *Chem. Engin. Sci.* **44**, 2781–2796 (1989).
 - [4] L. G. Leal, *Advanced transport phenomena: fluid mechanics and convective transport processes* (Cambridge University Press, 2007).
 - [5] Z. Neufeld and E. Hernandez-Garcia, *Chemical and biological processes in fluid flows: a dynamical systems approach* (World Scientific, 2009).
 - [6] L. Karp-Boss, E. Boss, and P.A. Jumars, “Nutrient fluxes to planktonic osmotrophs in the presence of fluid motion,” *Oceanogr. Marine Biol.* **34**, 71–108 (1996).
 - [7] U. Frisch, *Turbulence: the legacy of AN Kolmogorov* (Cambridge University Press, 1995).
 - [8] G. Falkovich, K. Gawędzki, and M. Vergassola, “Particles and fields in fluid turbulence,” *Rev. Mod. Phys.* **73**, 913 (2001).
 - [9] R. Margalef, “Life-forms of phytoplankton as survival alternatives in an unstable environment,” *Oceanol. Acta* **1**, 493–509 (1978).
 - [10] E. R. Abraham, “The generation of plankton patchiness by turbulent stirring,” *Nature* **391**, 577–580 (1998).
 - [11] C. López, Z. Neufeld, E. Hernandez-Garcia, and P. H. Haynes, “Chaotic advection of reacting substances: Plankton dynamics on a meandering jet,” *Phys. Chem. Earth, Part B* **26**, 313–317 (2001).
 - [12] J. R. Taylor and R. Stocker, “Trade-offs of chemotactic foraging in turbulent water,” *Science* **338**, 675–679 (2012).
 - [13] N. Desai, S. Dabiri, and A. M. Ardekani, “Nutrient uptake by chemotactic bacteria in presence of rising oil drops,” *Inter. J. Multiph. Flow* **108**, 156–168 (2018).
 - [14] M. M. Musielak, L. Karp-Boss, P. A. Jumars, and L. J. Fauci, “Nutrient transport and acquisition by diatom chains in a moving fluid,” *J. Fluid Mech.* **638**, 401–421 (2009).
 - [15] R. A. Lambert, F. Picano, W.-P. Breugem, and L. Brandt, “Active suspensions in thin films: nutrient uptake and swimmer motion,” *J. Fluid Mech.* **733**, 528–557 (2013).
 - [16] A. Sozza, F. Piazza, M. Cencini, F. De Lillo, and G. Boffetta, “Point-particle method to compute diffusion-limited cellular uptake,” *Phys. Rev. E* **97**, 023301 (2018).
 - [17] C. Pasquero, A. Bracco, and A. Provenzale, “Impact of the spatiotemporal variability of the nutrient

- flux on primary productivity in the ocean,” J. Geophys. Res.: Oceans **110** (2005).
- [18] G. K. Batchelor, “Mass transfer from a particle suspended in fluid with a steady linear ambient velocity distribution,” J. Fluid Mech. **95**, 369–400 (1979).
 - [19] N. A. Frankel and A. Acrivos, “Heat and mass transfer from small spheres and cylinders freely suspended in shear flow,” The Physics of Fluids **11**, 1913–1918 (1968).
 - [20] V. G. Levich, *Physicochemical Hydrodynamics* (Prentice-Hall, Englewood Cliffs, NJ, 1962).
 - [21] A. G. Lamorgese, D. A. Caughey, and S. B. Pope, “Direct numerical simulation of homogeneous turbulence with hyperviscosity,” Phys. Fluids **17**, 015106 (2005).
 - [22] L. Machiels, “Predictability of small-scale motion in isotropic fluid turbulence,” Phys. Rev. Lett. **79**, 3411 (1997).
 - [23] C. S. Peskin, “The immersed boundary method,” Acta Num. **11**, 479517 (2002).
 - [24] M. Galanti, D. Fanelli, S. D. Traytak, and F. Piazza, “Theory of diffusion-influenced reactions in complex geometries,” Phys. Chem. Chem. Phys. **18**, 15950–15954 (2016).
 - [25] A. Pal Singh Bhalla, B. E. Griffith, N. A. Patankar, and A. Donev, “A minimally-resolved immersed boundary model for reaction-diffusion problems,” J. Chem. Phys. **139**, 214112 (2013).
 - [26] N. Dorsaz, C. De Michele, F. Piazza, P. De Los Rios, and G. Foffi, “Diffusion-limited reactions in crowded environments,” Phys. Rev. Lett. **105**, 120601 (2010).
 - [27] M. O. Lavrentovich, J. H. Koschwanetz, and D. R. Nelson, “Nutrient shielding in clusters of cells,” Phys. Rev. E **87**, 062703 (2013).
 - [28] S. Chandrasekhar, “Stochastic problems in physics and astronomy,” Rev. Mod. Phys. **15**, 1 (1943).
 - [29] L. Biferale, “A note on the fluctuation of dissipative scale in turbulence,” Phys. Fluids **20**, 031703 (2008).
 - [30] D. Buaria, A. Pumir, E. Bodenschatz, and P. K. Yeung, “Extreme velocity gradients in turbulent flows,” New J. Phys. **21**, 043004 (2019).
 - [31] G. Brethouwer, J.C.R. Hunt, and F.T.M. Nieuwstadt, “Micro-structure and lagrangian statistics of the scalar field with a mean gradient in isotropic turbulence,” J. Fluid Mech. **474**, 193–225 (2003).
 - [32] S. A. Thorpe, *An introduction to ocean turbulence* (Cambridge University Press, 2007).
 - [33] R. G. Williams and M. J. Follows, *Ocean dynamics and the carbon cycle: Principles and mechanisms* (Cambridge University Press, 2011).
 - [34] A. Celani, G. Falkovich, A. Mazzino, and A. Seminara, “Droplet condensation in turbulent flows,” EPL **70**, 775 (2005).
 - [35] A. S. Lanotte, A. Seminara, and F. Toschi, “Cloud droplet growth by condensation in homogeneous isotropic turbulence,” J. Atmos. Sci. **66**, 1685–1697 (2009).
 - [36] Ch. Siewert, J. Bec, and G. Krstulovic, “Statistical steady state in turbulent droplet condensation,” J. Fluid Mech. **810**, 254–280 (2017).
 - [37] In particular, we used a forcing of the form $-\mu(\langle c \rangle(t) - c_0)$ which maintains, on average, a fixed mean concentration, thus replenishing the nutrient in a space homogeneous way, mimicking a large scale

injection.

- [38] R. Stocker, “Marine microbes see a sea of gradients,” *Science* **338**, 628–633 (2012).
- [39] G. K. Batchelor, “Mass transfer from small particles suspended in turbulent fluid,” *J. Fluid Mech.* **98**, 609–623 (1980).
- [40] E. A. Novikov, “Concerning a turbulent diffusion in a stream with a transverse gradient of velocity,” *J. Appl. Math. Mech.* **22**, 576–579 (1958).
- [41] D. E. Elrick, “Source functions for diffusion in uniform shear flow,” *Austral. J. Phys.* **15**, 283–288 (1962).